Divergolides T–W with Apoptosis-Inducing Activity from the Mangrove-Derived Actinomycete *Streptomyces* sp. KFD18

Li-Man Zhou [1,2,†], Fan-Dong Kong [2,†], Qing-Yi Xie [2], Qing-Yun Ma [2], Zhong Hu [3], You-Xing Zhao [2,*] and Du-Qiang Luo [1,*]

[1] College of Life Science, Key Laboratory of Medicinal Chemistry and Molecular Diagnosis of Ministry of Education, Hebei University, Baoding 071002, China; zhouliman88@126.com

[2] Hainan Key Laboratory for Research and Development of Natural Product from Li Folk Medicine, Institute of Tropical Bioscience and Biotechnology, Chinese Academy of Tropical Agricultural Sciences, Haikou 571101, China; kongfandong@itbb.org.cn (F.-D.K.); xieqingyi@itbb.org.cn (Q.-Y.X.); maqingyun@itbb.org.cn (Q.-Y.M.)

[3] Guangdong Provincial Key Laboratory of Marine Biotechnology, Department of Biology, Shantou University, Shantou 515063, China; hzh@stu.edu.cn

* Correspondence: zhaoyouxing@itbb.org.cn (Y.-X.Z.); duqiangluo@163.com (D.-Q.L.); Tel.: +86-139-5169-2350 (Y.-X.Z.)

† These authors contributed equally to this paper.

check for updates

Abstract: Four new ansamycins, named divergolides T–W (**1–4**), along with two known analogs were isolated from the fermentation broth of the mangrove-derived actinomycete *Streptomyces* sp. KFD18. The structures of the compounds, including the absolute configurations of their stereogenic carbons, were determined by spectroscopic data and single-crystal X-ray diffraction analysis. Compounds **1–4** showed cytotoxic activity against the human gastric cancer cell line SGC-7901, the human leukemic cell line K562, the HeLa cell line, and the human lung carcinoma cell line A549, with **1** being the most active while compounds **5** and **6** were inactive against all the tested cell lines. Compounds **1** and **3** showed very potent and specific cytotoxic activities (IC_{50} 2.8 and 4.7 μM, respectively) against the SGC-7901 cells. Further, the apoptosis-inducing effect of **1** and **3** against SGC-7901 cells was demonstrated by two kinds of staining methods for the first time.

Keywords: mangrove-derived actinomycete; ansamycins; divergolides; apoptosis-inducing activity

1. Introduction

Ansamycins are a class of bioactive macrolides that have been isolated from actinomycetes [1–4]. The most representatives of them are geldanamycin with HSP90 inhibitory activity [1], rifamycin with antibacterial activity [2], and maytansinoid with anticancer activity [3]. Divergolides represent a family of ansamycins with a 19-membered naphthalenic ansamacrolactam skeleton, which was first discovered from *Streptomyces* sp. HKI0576 and reported in 2011. Until now, a total of 19 members (divergolides A–S) of this family has been reported [5–7]. Many divergolides have shown cytotoxic and antibacterial activities [5–8].

As part our ongoing search for new bioactive secondary metabolites from marine microorganisms [9–12], *Streptomyces* sp. KFD18 attracted our attention for its ability to produce a series of metabolites with UV absorption bands around 275 and 305 nm, detected by HPLC analysis. Subsequent chemical investigations on the EtOAc extract from the fermentation broth of this strain led to the isolation and identification of four new ansamycins, named divergolides T–W (**1–4**), as well as

two known analogues 6,7-*epi*-24,25-dihydro-divergolide U (**5**) [8] and divergolide E (**6**) [7] (Figure 1). Herein, the structures and bioactivities of these compounds are reported.
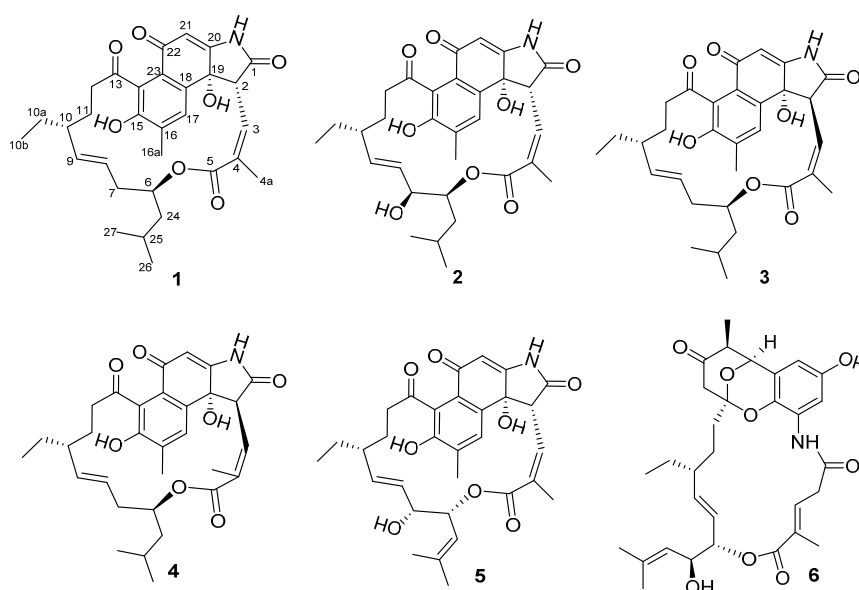

Figure 1. Structures of compounds **1**–**6**.

2. Results and Discussion

Compound **1** was obtained as a yellow crystal, and was found to have the molecular formula $C_{31}H_{37}NO_7$ from the HRESIMS *m/z* 536.2641 [M + H]$^+$. The UV spectrum showed characteristic absorption bands around 221 and 240 nm. The IR absorptions at 3414 and 1663 cm^{-1} revealed the presence of a hydroxy and carbonyl group, respectively. The ^1H and ^{13}C NMR spectra (Supplementary materials, Figures S2-1 and S2-2) along with the HSQC spectra (Supplementary materials, Figure S2-4) revealed the presence of five methyls, five sp^3 methylenes, nine methines (including five sp^2 and one oxygenated sp^3), twelve non-protonated carbons (including two ketone carbonyls, two ester or amide carbonyls, seven aromatic or olefinic carbons, and one hydroxylated carbon). Comparison of the above data with those of the known analogue **5** [8] suggested that their planar structures were quite similar, except that the hydroxy at C-7 was absent, and the Δ^{24} double bond of **5** was hydrogenated in **1**. In the ^1H-^1H COSY spectrum (Figure 2) of **1**, correlations of H-26/H-25/H-27 and H-25/H-24/H-6/H-7 were observed, which further confirmed the above deduction. The remaining substructure of **1** was found to be identical to that of **5** by analysis of the 2D NMR data.
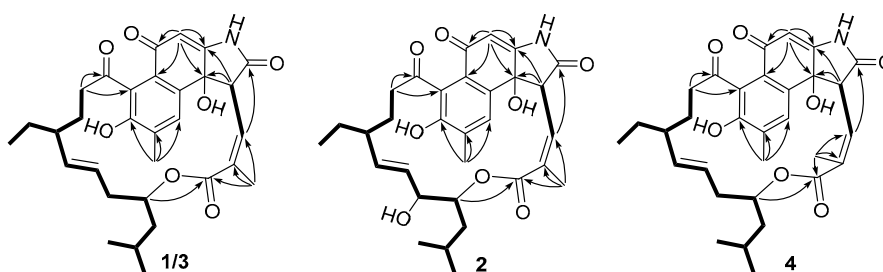

Figure 2. Key COSY (—) and HMBC (→) correlations of **1**–**4**.

The large *J* value (15.6 Hz) of H-8/H-9 (Table 1) suggested the *E* configuration of the Δ^8 double bond, while the relative downfield shift ($\delta_{C/H}$ 21.4/2.17) of the allylic methyl C-4a [13] and ROESY cross-peak (Figure 3) between H-4a and H-3 (δ_H 6.60) suggested the *Z* configuration of the Δ^3 double bond. Additionally, in the ROESY spectrum (Figure 3), correlations of H-10/H-8/H-24/H-2 and

H-9/H-10a led to the assignment of the full relative configuration of compound **1,** as shown in Figure 3. To support the above assignment and determine the absolute configuration of **1**, a single-crystal X-ray diffraction pattern was obtained using the anomalous scattering of Cu Kα radiation (Figure 4), allowing an explicit assignment of the absolute structure as 2*R*, 6*S*, 10*R*, and 19*R* based on the Flack parameter of −0.05(8).
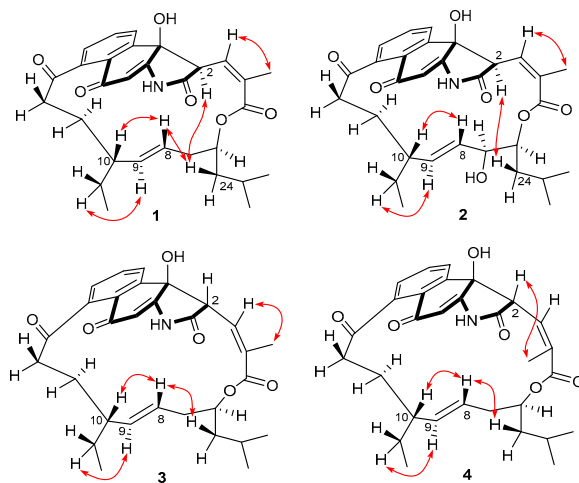

Figure 3. Key ROESY correlations of **1–4**.

Table 1. ^{13}C NMR data for **1–4** in CD$_3$OD.

Position	1	2	3	4
	δ_C	δ_C	δ_C	δ_C
1	177.2, C	177.1, C	177.2, C	176.8, C
2	55.2, CH	55.3, CH	55.8, CH	55.3, CH
3	131.7, CH	132.9, CH	126.7, CH	132.5 CH
4	136.8, C	136.1, C	138.4, C	135.0, C
4a	22.0, CH$_3$	22.1, CH$_3$	21.4, CH$_3$	13.5, CH$_3$
5	168.0, C	167.7, C	169.5, C	167.9, C
6	74.6, CH	76.7, CH	74.5, CH	74.0, CH
7	36.1, CH$_2$	70.5, CH	36.6, CH$_2$	36.3, CH$_2$
8	125.1, CH	128.2, CH	126.3, CH	125.3, CH
9	139.6, CH	136.1, CH	138.8, CH	138.6, CH
10	46.0, CH	45.9, CH	44.2, CH	43.2, CH
10a	26.9, CH$_2$	27.0, CH$_2$	29.3, CH$_2$	25.6, CH$_2$
10b	13.2, CH$_3$	13.2, CH$_3$	12.7, CH$_3$	11.1, CH$_3$
11	31.7, CH$_2$	31.5, CH$_2$	34.8, CH$_2$	31.6, CH$_2$
12	40.5, CH$_2$	40.5, CH$_2$	42.5, CH$_2$	42.0, CH$_2$
13	212.4, C	212.4, C	212.1, C	212.1, C
14	130.1, C	130.2, C	127.8, C	130.6, C
15	153.5, C	153.5, C	153.4, C	152.9, C
16	132.6, C	132.9, C	133.1, C	133.4, C
16a	17.0, CH$_3$	17.0, CH$_3$	17.0, CH$_3$	16.9, CH$_3$
17	130.8, CH	130.8, CH	132.8, CH	131.9, CH
18	134.3, C	136.1, C	134.3, C	135.0, C
19	73.7, C	73.8, C	73.6, C	75.2, C
20	164.8, C	164.7, C	164.6, C	164.6, C
21	103.9, CH	104.0, CH	103.4, CH	104.3, CH
22	185.4, C	185.4, C	185.7, C	185.7, C
23	129.8, C	129.9, C	130.4, C	130.6, C
24	42.6, CH$_2$	38.4, CH$_2$	41.5, CH$_2$	41.9, CH$_2$
25	25.5, CH	25.7, CH	25.3, CH	25.6, CH
26	22.7, CH$_3$	22.2, CH$_3$	22.1, CH$_3$	22.4, CH$_3$
27	23.0, CH$_3$	23.8, CH$_3$	23.7, CH$_3$	23.6, CH$_3$

Compound **2** was determined to have a molecular formula of $C_{31}H_{37}NO_8$ based on HRESIMS data, with one oxygen atom more than that of **1**. The UV spectrum of **2** was nearly identical to that of **1**, suggesting that **2** was a homologue of **1**. Their NMR data (Tables 1 and 2) were also quite similar, except for the replacement of CH_2-7 signals in **1** by signals for a hydroxylated sp^3 methine ($\delta_{C/H}$ 70.5/3.90) in **2**. In the COSY spectrum (Supplementary materials, Figure S3-6), correlations of this hydroxylated sp^3 methine with H-8 (δ_H 4.06) and H-6 (δ_H 4.99) were observed, further confirming that CH_2-7 in **1** was oxidized to a hydroxylated methine in **2**. The similar *J* values (Table 1) and ROESY data (Figure 3) between **1** and **2** suggested that both compounds had the same configuration at the stereogenic centers C-2, C-6, C-10, and C-19 and double bonds Δ^3 and Δ^8. The syn orientation between H-6 and H-7 was deduced from their small vicinal coupling constant (*J* = 2.6 Hz) [12].
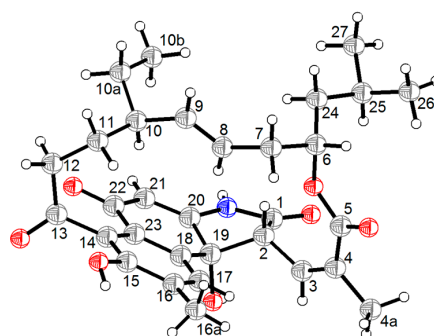

Figure 4. ORTEP diagram of **1**.

Table 2. ^{1}H NMR data for **1–4** in CD_3OD.

Position	1	2	3	4
	δ_H (*J* in Hz)	δ_H (*J* in Hz)	δ_H (*J* in Hz)	δ_H (*J* in Hz)
2	4.74, d (10.9)	4.84, d (10.6)	4.09, d (10.9)	4.06, d (8.4)
3	6.60, dq (10.9, 1.6)	6.67, dq (10.6, 1.6)	6.36, dq (10.8, 1.6)	5.89, dq (8.4, 1.6)
4a	2.20, d (1.6)	2.21, d (1.6)	2.17, d (1.6)	2.08, d (1.0)
6	5.05, m	4.99, m	5.04, m	4.87, m
7	1.96, m	3.90, ddd (2.74, 2.6, 2.6)	2.15, m	2.25, m
	2.15, m		2.15, m	2.14, m
8	3.93, ddd (15.3, 10.2, 3.6)	4.06, dd (15.6, 2.8)	3.78, ddd (15.6, 6.0, 6.0)	4.77, ddd (15.6, 9.1, 4.9)
9	5.01, dd (15.3, 9.3)	5.24, dd (15.6, 9.3)	4.87, dd (15.6, 9.4)	5.24, dd (15.6, 7.7)
10	1.32, overlap	1.37, overlap	1.46, overlap	1.78, m
10a	0.89, m	0.92, m	1.02, m	1.43, overlap
	0.89, m	1.49, overlap	1.34, overlap	1.18, overlap
10b	0.66, t (7.4)	0.65, t (7.4)	0.73, t (7.4)	0.77, t (7.5)
11	1.35, m	1.37, overlap	1.68, m	1.29, overlap
	1.46, overlap	1.49, overlap	1.25, m	1.57, m
12	2.61, m	2.62, m	2.64, ddd (14.0, 11.3, 2.8)	2.46, m
	2.90, m	2.99, m	2.46, ddd (14.0, 7.4, 2.9)	2.77, m
16a	2.22, s	2.21, s	2.30, s	2.31, s
17	7.41, s	7.38, s	7.57, s	7.28, s
21	5.82, s	5.82, s	5.80, s	5.85, s
24	1.13, m	1.14, m	1.15, m	1.20, overlap
	1.32, overlap	1.31, overlap	1.32, overlap	1.30, overlap
25	1.46, overlap	1.49, overlap	1.47, overlap	1.45, overlap
26	0.81 d (6.6)	0.83 d (6.6)	0.88 d (6.5)	0.88 d (6.6)
27	0.81, d (6.6)	0.79, d (6.6)	0.82, d (6.5)	0.83, d (6.6)

Compounds **3** and **4** had the same molecular formula of $C_{31}H_{37}NO_7$ as that of **1**. The ^{1}H and ^{13}C NMR data (Supplementary materials, Figures S4-1, S4-2, S5-1, and S5-2) of **3** and **4** were also quite similar to those of **1**. Detailed analysis of the ^{1}H-^{1}H COSY and HMBC data (Supplementary materials, Figures S4-5, S4-6, S5-5, and S5-6) of **3** and **4** revealed the same H/H and H/C correlational relationship as those of **1**, indicating that **3** and **4** shared the same planar structure with **1**. However, unlike the ROESY data of **1** and **2**, the absence of correlations (Supplementary materials, Figures S4-7 and S5-7) between H-2 and H-24 (δ_H 1.15 and 1.20, respectively) in **3** and **4** revealed the H-2 protons had opposite orientations as compared to those of **1** and **2**. The syn orientation of H-2 and OH-19 in **3** and **4** was deduced by comparison of the NMR data with those of hygrocins D and F [13]. The above assignment was further supported by the phenomenon that H-2 signals (δ_H 6.36 and 5.89, respectively) of **3** and **4** resonated upfield [13] compared to those (δ_H 6.60 and 6.67, respectively) of **1** and **2**. Further, in the ROESY spectra (Figure 3), correlations of H-4a/H-3 of **3** while H-4a/H-2 of **4** were observed, revealing the *Z* and *E* configuration of Δ^3 double bond in **3** and **4**, respectively.

Compounds **1**–**6** were tested for their cytotoxic activity against the human gastric cancer cell line SGC-7901, the human leukemic cell line K562, the HeLa cell line, and the human lung carcinoma cell line A549. The results (Table 3) showed that compounds **1**–**4** exhibited cytotoxic activity against SGC-7901 (IC_{50} = 2.8, 9.8, 4.7, and 20.9 μM, respectively), K562 (IC_{50} = 6.6, 9.0, 7.6, and 16.3 μM, respectively), HeLa (IC_{50} = 9.6, >50, 14.1, and 29.5 μM, respectively), and A549 (IC_{50} = 14.9, 24.7, 20.9, and 33.2 μM, respectively) cell lines, with **1** being the most active while compounds **5** and **6** were inactive against all the tested cell lines. The above data showed that hydroxylation at C-7 or inversion of the configuration at C-2 or Δ^3 double bond in compound **1** could significantly reduce cytotoxic activity.

Table 3. Cytotoxic activities of compounds **1**–**6**.

Compound	IC_{50} (μM)			
	SGC-7901	**K562**	**Hela**	**A549**
1	2.8	6.6	9.6	14.9
2	9.8	9.0	>50	24.7
3	4.7	7.6	14.1	20.9
4	20.9	16.3	29.5	33.2
5	>50	>50	>50	>50
6	>50	>50	>50	>50
Imatinib	86.8	0.2	18.8	45.6
Adriamycin	6.9	10.7	11.4	5.5

In order to determine whether the compounds could induce apoptosis, we used two kinds of staining methods. Double staining with acridine orange-ethidium bromide (AOEB) allows for differentiation of live, apoptotic, and necrotic cells [14]; live cells have green, regular-sized nuclei. Green or yellow-green nuclear condensation or fragmentation identifies early apoptotic cells, and orange or red staining identifies late apoptotic or necrotic cells. DAPI staining can reveal the typical apoptotic feature: a condensed nucleus and apoptotic body formation [15]. After SGC-7901 cells were cultured with compounds **1** and **3** at double the IC_{50} concentration for 48 h. AOEB staining showed us that the cells were dyed yellow-green or orange. DAPI staining showed that many cells had typical apoptotic features (Figure 5). All staining results indicated that compounds **1** and **3** had apoptosis-inducing activity against SGC-7901. The apoptosis-inducing activity of divergolides has been reported for the first time.
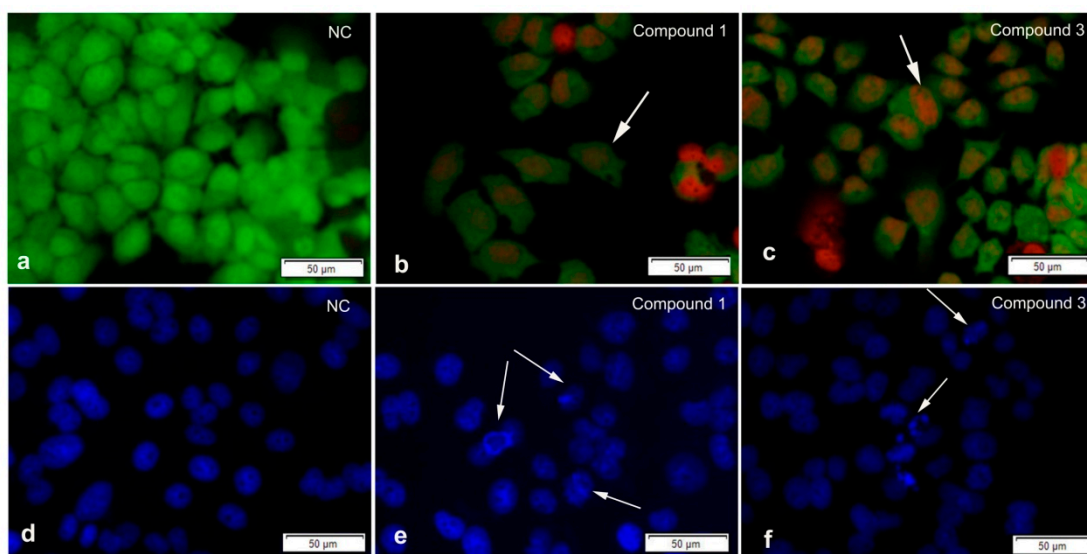
Figure 5. The staining results of compounds **1** and **3** on SGC-7901. Acridine orange-ethidium bromide (AOEB) staining on SGC-7901 cells at 48 h after compound addition (**a**–**c**). DAPI staining on SGC-7901 cells at 48 h after compound addition (**d**–**f**). The concentrations of compounds **1** and **3** were 5.6 μM and 9.4 μM, respectively. NC: Negative control, DMSO of the same volume.

3. Experimental Section

3.1. General Experimental Procedure

Optical rotations were measured with a JASCO P-1020 digital polarimeter. The IR spectra were obtained with a Nicolet Nexus 470 spectrophotometer as KBr discs. The UV spectra were obtained with a Beckman DU 640 spectrophotometer. The NMR spectra were recorded on a Bruker AV-500 spectrometer, with a CD_3OD solvent peak signal as the chemical shift reference. All compounds isolated underwent NMR analysis using about 500 μL CD_3OD solvent. HREIMS data were acquired on a Micromass Autospec-Ultima-TOF, API QSTAR Pulsar 1, or Waters Autospec Premier spectrometer. Semi-preparative HPLC separation used octadecyl silane (ODS) columns (YMC-pack ODS-A, 10 × 250 mm, 5 μm, 4 mL/min) for separation. Thin-layer chromatography (TLC) and column chromatography (CC) were carried out on precoated silica gel GF_{254} (10–40 μm, Qingdao Marine Chemical Inc., Qingdao, China) and silica gel (200–300 mesh, Qingdao Marine Chemical Inc., Qingdao, China), respectively.

3.2. Strain and Fermentation

The strain *Streptomyces* sp. KFD18 was isolated from Mangrove sediment, collected from Danzhou, Hainan province, in China, which was identified based on the 16S rRNA gene sequences (GenBank accession No. MK478900, Supporting Information) of the single colonies. A reference culture of *Streptomyces* sp. KFD18 was deposited in our laboratory and was maintained at −80 °C. *Streptomyces* sp. KFD18 was cultured in seawater medium containing 1% starch, 0.1% peptone, and 0.2% $CaCO_3$ on a rotary shaker (180 rpm) at 28 °C for 4 d to afford a seed culture. Fermentation (30 L) was performed using the same medium on a rotary shaker (180 rpm) at 28 °C for 10 d.

3.3. Extraction and Isolation

The fermented cultures were extracted with three-fold volumes of EtOAc, then the EtOAc solutions were combined and evaporated under reduced pressure to produce a dark brown, solid, crude extract (2.9 g). The extract was fractionated by a silica gel VLC column using different solvents of increasing polarity, from MeOH/H_2O (1:4) to MeOH/H_2O (1:0), to yield seven fractions (Frs. 1−7). Fr. 5 (87 mg) was subjected to semipreparative HPLC (YMC-pack ODS-A, 5 μm; 10 × 250 mm;

50% MeCN/H_2O; containing 0.1% TFA; 4 mL/min) to afford compounds **1** (t_R 19.4 min; 14.2 mg) and **4** (t_R 23.4 min; 4.3 mg). Fr. 6 (264 mg) was subjected to semipreparative HPLC (YMC-pack ODS-A, 5 μm; 10 × 250 mm; 70% MeCN/H_2O; containing 0.1% TFA; 4 mL/min) to afford compound **3** (t_R 13.1 min; 6.4 mg). Fr. 4 (124 mg) was purified by semipreparative HPLC (YMC-pack ODS-A, 5 μm; 10 × 250 mm; 40% MeCN/H_2O; containing 0.1% TFA; 4 mL/min) to afford compound **2** (t_R 9.6 min; 3.1 mg) and compound **5** (t_R 11.3 min; 7.7 mg). Fr. 3 (214 mg) was purified by Sephadex LH-20 chromatography and eluted with MeOH to afford compound **6** (13.8 mg)

Divergolide T (**1**): Colorless crystal; $[\alpha]_D^{25}$ −190 (*c* 0.1, MeOH); UV (MeOH) λ_{max} (log ε): 305.0 (3.70), 275.0 (3.68) nm; IR (KBr) ν_{max} (cm^{-1}): 3414, 2957, 2855, 1663, 1573, 1194, and 1144. ^{1}H and ^{13}C NMR data, Tables 1 and 2; HRESIMS *m/z* 536.2641 [M + H]$^+$ (calculated for $C_{31}H_{38}O_7N$, 536.2643).

Divergolide U (**2**): White powder; $[\alpha]_D^{25}$ +60 (*c* 0.1, MeOH); UV (MeOH) λ_{max} (log ε): 305.0 (3.72), 275.0 (3.69) nm; IR (KBr) ν_{max} (cm^{-1}): 3444, 2925, 2855, 1677, 1442, 1199, and 1141. ^{1}H and ^{13}C NMR data, Tables 1 and 2; HRESIMS *m/z* 550.2438 [M − H]$^+$ (calculated for $C_{31}H_{36}O_8N$, 550.2446).

Divergolide V (**3**): White powders; $[\alpha]_D^{25}$ +118 (*c* 0.1, MeOH); UV (MeOH) λ_{max} (log ε): 305.0 (3.75), 275.0 (3.70) nm; IR (KBr) ν_{max} (cm^{-1}): 3413, 2926, 1649, 1583, 1334, 1243, 1146, and 1058. ^{1}H and ^{13}C NMR data, Tables 1 and 2; HRESIMS *m/z* 536.2640 [M + H]$^+$ (calculated for $C_{31}H_{38}O_7N$, 536.2643).

Divergolide W (**4**): White powders; $[\alpha]_D^{25}$ +72 (*c* 0.1, MeOH); UV (MeOH) λ_{max} (log ε): 305.0 (3.68), 275.0 (3.66) nm; IR (KBr) ν_{max} (cm^{-1}): 3442, 2926, 2961, 1673, 1577, 1199, and 1138. ^{1}H and ^{13}C NMR data, Tables 1 and 2; HRESIMS *m/z* 534.2490 [M − H]$^-$ (calculated for $C_{31}H_{36}O_7N$, 534.2497).

X-ray Crystal Data for 1: Colorless crystals of **1** were obtained in the mixed solvent of MeOH. Crystal data of **1** were obtained on a Bruker D8 QUEST diffractometer (Bruker) with graphite monochromated Cu Kα radiation (λ = 1.54178 Å). Crystallographic data for **1** were deposited in the Cambridge Crystallographic Data Center as supplementary publication number CCDC 1893418. These data can be obtained free of charge from The Cambridge Crystallographic Data Centre via www.ccdc.cam.ac.uk/data_request/cif.

Crystal data for **1**. Monoclinic, $C_{31}H_{37}NO_7$; space group P 1 21 1 with *a* = 12.5723(5) Å, *b* = 14.6723(6) Å, *c* = 17.4900(8) Å, *V* = 3226.3(2) Å^3, Z = 1, D_{calcd} = 1.109 g/cm^3, μ = 0.691 mm^{-1}, and *F*(000) = 1077. *T* = 296.15 K. R1 = 0.0526 (*I* > 2σ(I)), *wR2* = 0.1480 (all data), *S* = 1.021. Absolute structure parameter: −0.05(8). The structures were solved using ShelXS. The structural solutions were found by direct methods and refined using the ShelXL package by least squares minimization. The final structures were examined using the Addsym subroutine of PLATON to assure that no additional symmetry could be applied to the models. All non-hydrogen atoms were refined with anisotropic thermal factors.

3.4. Bioassays for Cytotoxic and Apoptosis-Inducing Activity

The cytotoxic activities of compounds **1–6** were tested in vitro by using the MTT method optimized by Chuan et al. [16]. Imatinib and adriamycin were used as the positive controls, and a medium with 4‰ DMSO was used as the negative control in the bioassay test. For AOEB staining, SGC-7901 cells were cultured in 96-well cell culture plates. After 48 h incubation, the culture medium was removed and washed with PBS three times. AO and EB were added to a final concentration of 2 μg/mL each. For DAPI staining, cells were fixed with 4% paraformaldehyde solution for 10 min, incubated with 0.1% TritonX-100 on ice for 30 min, and then washed with PBS three times. DAPI was added to a final concentration of 1 μg/mL each. The pictures were taken using a fluorescence microscope.

4. Conclusions

In conclusion, four new ansamycins (**1–4**) and two known analogs (**5** and **6**) were isolated from the fermentation broth of mangrove-derived actinomycete *Streptomyces* sp. KFD18. Compounds **1–4**

exhibited cytotoxic activity against SGC-7901(IC_{50} = 2.8, 9.8, 4.7, and 20.9 μM, respectively), K562 (IC_{50} = 6.6, 9.0, 7.6, and 16.3 μM, respectively), HeLa (IC_{50} = 9.6, >50, 14.1, and 29.5 μM, respectively), and A549 (IC_{50} = 14.9, 24.7, 20.9, and 33.2 μM, respectively) cell lines, with **1** being the most active while compounds **5** and **6** were inactive against all the tested cell lines. The two most active compounds, **1** and **3,** could induce apoptosis of SGC-7901 cells.

Supplementary Materials: The following are available online at http://www.mdpi.com/1660-3397/17/4/219/s1, Figures S1–S5-9: HRESIMS, IR and 2D NMR spectra of the new compounds **1**–**4**, and the 16S rRNA gene sequence of *Streptomyces* sp. KFD18 are supplied.

Author Contributions: L.-M.Z. contributed to the fermentation, compound purification, and the bioassay. F.-D.K. was responsible for structural elucidation and preparation of the paper. Q.-Y.X. contributed to Actinomycete strain isolation. Q.-Y.M. identified the strain. Y.-X.Z. and D.-Q.L. designed the work and revised the paper.

Conflicts of Interest: The authors declare no conflict of interest.

References

1. Fukuyo, Y.; Hunt, C.R.; Horikoshi, N. Geldanamycin and its anti-cancer activities. *Cancer Lett.* **2010**, *290*, 24–35. [CrossRef] [PubMed]

2. Floss, H.G.; Yu, T.W. Rifamycin mode of action, resistance, and biosynthesis. *Chem. Rev.* **2005**, *105*, 621–632. [CrossRef] [PubMed]

3. Cassady, J.M.; Chan, K.K.; Floss, H.G.; Leistner, E. Recent developments in the maytansinoid antitumor agents. *Chem. Pharm. Bull.* **2004**, *52*, 1–26. [CrossRef] [PubMed]

4. Higashide, E.; Asai, M.; Ootsu, K.; Tanida, S.; Kozai, Y.; Hasegawa, T.; Kishi, T.; Sugino, Y.; Yoneda, M. Ansamitocin, a group of novel maytansinoid antibiotics with antitumour properties from Nocardia. *Nature* **1977**, *270*, 721–722. [CrossRef] [PubMed]

5. Ding, L.; Maier, A.; Fiebig, H.H.; Görls, H.; Lin, W.H.; Peschel, G.; Hertweck, C. Divergolides A–D from a mangrove endophyte reveal an unparalleled plasticity in ansa-macrolide biosynthesis. *Angew. Chem.* **2011**, *123*, 1668–1672. [CrossRef]

6. Ding, L.; Franke, J.; Hertweck, C. Divergolide congeners illuminate alternative reaction channels for ansamycin diversification. *Org. Biomol. Chem.* **2015**, *13*, 1618–1623. [CrossRef] [PubMed]

7. Xu, Z.; Baunach, M.; Ding, L.; Peng, H.; Franke, J.; Hertweck, C. Biosynthetic code for divergolide assembly in a bacterial mangrove endophyte. *ChemBioChem* **2014**, *15*, 1274–1279. [CrossRef] [PubMed]

8. Zhao, G.; Li, S.; Guo, Z.; Sun, M.; Lu, C. Overexpression of div 8 increases the production and diversity of divergolides in *Streptomyces* sp. W112. *RSC Adv.* **2015**, *5*, 98209–98214. [CrossRef]

9. Kong, F.D.; Ma, Q.Y.; Huang, S.Z.; Wang, P.; Wang, J.F.; Zhou, L.M.; Yuan, J.Z.; Dai, H.F.; Zhao, Y.X. Chrodrimanins K-N and related meroterpenoids from the fungus *Penicillium* sp. SCS-KFD09 isolated from a marine worm, *Sipunculus nudus*. *J. Nat. Prod.* **2017**, *80*, 1039–1047. [CrossRef] [PubMed]

10. Kong, F.D.; Zhang, R.S.; Ma, Q.Y.; Xie, Q.Y.; Wang, P.; Chen, P.W.; Zhou, L.M.; Dai, H.F.; Luo, D.Q.; Zhao, Y.X. Chrodrimanins O–S from the fungus *Penicillium* sp. SCS-KFD09 isolated from a marine worm, *Sipunculusnudus*. *Fitoterapia* **2017**, *122*, 1–6. [CrossRef] [PubMed]

11. Kong, F.D.; Huang, X.L.; Ma, Q.Y.; Xie, Q.Y.; Wang, P.; Chen, P.W.; Zhou, L.M.; Yuan, J.Z.; Dai, H.F.; Luo, D.Q. Helvolic acid derivatives with antibacterial activities against *Streptococcus agalactiae* from the marine-derived fungus *Aspergillus fumigatus* HNMF0047. *J. Nat. Prod.* **2018**, *81*, 1869–1876. [CrossRef] [PubMed]

12. An, C.L.; Kong, F.D.; Ma, Q.Y.; Xie, Q.Y.; Yuan, J.Z.; Zhou, L.M.; Dai, H.F.; Yu, Z.F.; Zhao, Y.X. Chemical Constituents of the Marine-Derived Fungus *Aspergillus* sp. SCS-KFD66. *Mar. Drugs* **2018**, *16*, 468. [CrossRef] [PubMed]

13. Lu, C.; Li, Y.; Deng, J.; Li, S.; Shen, Y.; Wang, H.; Shen, Y. Hygrocins C–G, cytotoxic naphthoquinone ansamycins from gdmAI-disrupted *Streptomyces* sp. LZ35. *J. Nat. Prod.* **2013**, *76*, 2175–2179. [CrossRef] [PubMed]

14. Braun, J.S.; Novak, R.; Murray, P.J.; Eischen, C.M.; Susin, S.A.; Kroemer, G.; Halle, A.; Weber, J.R.; Tuomanen, E.I.; Cleveland, J.L. Apoptosis-inducing factor mediates microglial and neuronal apoptosis caused by pneumococcus. *J. Infect. Dis.* **2001**, *184*, 1300–1309. [CrossRef] [PubMed]

15. Yuan, Z.F.; Tang, Y.M.; Xu, X.J.; Li, S.S.; Zhang, J.Y. 10-Hydroxycamptothecin induces apoptosis in human neuroblastoma SMS-KCNR cells through p53, cytochrome c and caspase 3 pathways. *Neoplasma* **2016**, *63*, 72–79. [CrossRef] [PubMed]

16. Chen, C.; Liang, F.; Chen, B.; Sun, Z.Y.; Xue, T.D.; Yang, R.L.; Luo, D.Q. Identification of demethylincisterol A3 as a selective inhibitor of protein tyrosine phosphatase Shp2. *Eur. J. Pharmacol.* **2017**, *795*, 124–133. [CrossRef] [PubMed]